Journal of Thermal Analysis and Calorimetry, Vol. 57 (1999) 433-445

ON THE OXIMINE COMPLEXES OF TRANSITION METALS
Part 110: Spectroscopic and DSC study on some $[Fe(Diox{\cdot}H)_2L_2]$ and $[Fe(Diox)_3(BOR)_2]$ type chelates and clathrochelates*

L. Nagy[1], *J. Zsakó*[2], *Cs. Novák*[3], *Cs. Várhelyi*[2], *Gy. Vankó*[4] *and G. Liptay*[5]

[1]Department of Inorganic and Analytical Chemistry, József Attila University, H-6701 Szeged, P. O. Box 440, Hungary
[2]Department of Natural Sciences and Mathematics, Transylvanian Museum Association Cluj, Romania
[3]Research Group for Technical Analytical Chemistry of the Hungarian Academy of Sciences Technical University of Budapest
[4]Department of Nuclear Chemistry, Eötvös University, Budapest
[5]Department of Inorganic Chemistry, Technical University of Budapest, H-1521 Hungary

Abstract

A number of 15 $[Fe(Diox{\cdot}H)_2L_2]$ type chelates and $[Fe(Diox)_3(BOR)_2]$ clathrochelates ($Diox{\cdot}H_2$ – dimethylglyoxime, glyoxime, propoxime, nyoxime, furyl-dioxime; *L*-pyridine, alkyl-pyridine derivatives, diethyl-phenyl-phosphine, diethyl-*p*-tolyl-phosphine) were obtained and characterized by means of far and middle FTIR and Mössbauer spectroscopic methods. Some structural problems were discussed on the basis of the optical data.

The DSC measurements show the higher thermal stability of the clathrochelates without O–H···O intramolecular hydrogen bonds (with asymmetric octahedral structure), as compared to the $[Fe(Diox{\cdot}H)_2L_2]$ *trans*, symmetric chelates containing O–H···O bonds. The kinetic parameters of the thermal decomposition of the complexes have been derived using the nomogram method.

Keywords: DSC, iron(II)-oxime complexes, kinetic parameters, Mössbauer spectroscopy

Introduction

The iron(II) salts form reddish coloured solutions with α-dioximes. The iron(II) complexes of this type can be obtained very difficulty in solid, crystalline state, generally, in not well defined stochiometric composition {e.g. $2NaFe(DH)_2(OH)$+approx. $1Fe(DH)_2$} [1–4].

If aromatic and heterocyclic organic N-bases or tertiary phosphines are present in the iron(II)-α-dioxime system, sparingly soluble, characteristic crystalline compounds can be isolated [5].

* Presented at ESTAC-7, Balatonfüred, Hungary

1418–2874/99/ $ 5.00

Akadémiai Kiadó, Budapest
Kluwer Academic Publishers, Dordrecht

The diamagnetic properties of the hexa-co-ordinated mixed chelates: $[Fe(Diox{\cdot}H_2)L_2]$ prove the presence of Fe(II) in their composition. The solubility, thermal stability and some physico-chemical properties of these derivatives are influenced by the nature of the chelating agent and of the monodentate *L*-ligands.

In basic media, in the presence of BF_3, boric acid and borate esters (in anhydrous alcohol), the reaction of FeX_2 (X=Cl^{-1}, Br^{-1}) with α-dioximes leads to the formation of clathrochelates of the type: $Fe(Diox)_3(BOR)_2$ [6–9].

Results and discussion

Using aliphatic – [glyoxime, dimethylglyoxime, propoxime (methyl-isopropyl-2,3-dione dioxime)], alicyclic – [1,2-cyclohexane dione dioxime (nyoxime)] and

Table 1 $[Fe(Diox)_3L_2]$ chelates and $[Fe(Diox)_3(BOR)_3]$ clathrochelates

Formula	$M_{calc.}$	Aspect	Anal.	calc.	found
$[Fe(Glyox{\cdot}H)_2(\gamma\text{-picoline})_2]{\cdot}H_2O$	451.2	redbrown rhomb. plates	Fe N	12.9 19.5	13.1 19.2
$[Fe(Glyox{\cdot}H)_2(3,4\text{-lutidine})_2]{\cdot}H_2O$	459.2	redbrown prisms	Fe N	12.2 18.3	12.0 18.6
$[Fe(DH)_2(benzimidazole)_2]$	524.3	reddish violet crops	Fe N	10.6 21.4	12.0 18.6
$[Fe(DH)_2(Et_2Ph{\cdot}P)_2]$	618.4	goldbrown plates	Fe	9.0	9.1
$[Fe(DH)_2(Et_2(p\text{-tolyl})P)_2]$	644.5	goldbrown desks	Fe N	8.6 8.7	8.5 8.4
$[Fe(Propox{\cdot}H)_2(\beta\text{-picoline})_2]$	528.4	reddish brown plates	Fe N	10.6 15.9	10.4 16.2
$[Fe(Propox{\cdot}H)_2(\gamma\text{-picoline})_2]$	528.4	irregular brown plates	Fe N	10.6 15.9	10.4 16.2
$[Fe(Propox{\cdot}H)_2(Et_2Ph{\cdot}P)_2]$	674.6	brown rhomb. prisms	Fe N	8.3 8.3	8.7 8.3
$[Fe(Propox{\cdot}H)_2(Et_2(p\text{-tolyl})P)_2]$	708.6	irregular brown prisms	Fe N	7.9 7.9	8.1 7.6
$[Fe(Furox{\cdot}H)_2(Et_2Ph{\cdot}P)_2]{\cdot}H_2O$	826.6	brown irregular prisms	Fe N	6.7 6.8	6.9 6.6
$[Fe(Furox{\cdot}H)_2(Et_2(p\text{-tolyl})P)_2]$	852.6	short brown prisms	Fe N	6.5 6.6	6.4 6.8
$[Fe(D)_3(BOCH_3)_2]{\cdot}H_2O$	500	orange brown plates	Fe N	11.8 16.8	11.6 16.6
$[Fe(D)_3(BOH)_2]{\cdot}4H_2O$	513	orange brown cubic cryst.	Fe N	10.9 16.3	11.3 15.9
$[Fe(Niox)_3(BOH)_2]{\cdot}4H_2O$	606	dark orange prisms	Fe	9.2	9.4
$[Fe(Niox)_3(BOCH_3)_2]$	562.8	sparkling orange brown trigonal prism	Fe	9.9	10.1

heterocyclic dioximes [α-furyldioxime] for the synthesis of chelates and clathrochelates of the above mentioned types, 15 compounds were obtained and characterized (Table 1).

The middle and far FTIR spectra of these compounds show that the $[Fe(Diox{\cdot}H_2)L_2]$ nonelectrolytic compounds have a symmetric *(trans)* geometric structure, stabilized in the equatorial plane with two short intramolecular O–H···O hydrogen bridges (ν_{O-H}: 2360–2400 cm^{-1}, $\delta_{O-H\cdots O}$: 1700–1800 cm^{-1} (w)).

The clathrochelates have an asymmetric distorted octahedral structure with encapsulated boron containing ligands, without hydrogen bonding.

Table 2 FTIR spectral data on some $[Fe(Diox)_3L_2]$ chelates and $[Fe(Diox)_3(BOR)_3]$ clathrochelates

Vibration	Frequency/cm^{-1}					
	I	II	III	IV	V	VI
νO–H	3300– 3100	–	–	–	3400–3200s 3100s	–
νC–H	–	2950m 2840m	2960m 2850m	2950m 2860m	–	2960s 2860s
νC–H	2340– 2380m	2330– 2400m	2350– 2400m	2350– 2400m	–	–
δO–H···O	1700– 1780w	1720w 1800w	1720w 170w	1730w 1800w	–	–
δH_2O	1620m	–	–	–	1630s	–
νC=N	1570s	1560s	1530s	1560m	1570s	1560s
δCH_2	–	1450s 1380s	1440s 1370s	1460s 1360s	–	1450s 1380s
νN–O	1230s 1090s	1225s 1100s	1230s 1100s	1230s 1120s	1235s 1105s	1235s 1090s
νB–O	–	–	–	–	1060s 1010s 800s	1030s 1000m 800m
γC–H	–	770	740s	760m	–	–
$\nu Fe–N_{(oxim)}$	510s	505s	510m	510m	510m	505m
$\nu Fe–N_{(amine)}$	480s	485s	–	–	–	–
νFe–P	–	–	410m	410m	–	–
$\delta N_{ox}–Fe–N_{ox}$	330s	325s	320s	3210s	315s	320s
$\delta N_{am}–Fe–N_{am}$	280s	270s	–	–	–	–

I $[Fe(Glyox{\cdot}H)_2(\gamma\text{-picoline})_2]{\cdot}H_2O$; II $[Fe(Propox{\cdot}H)_2(\beta\text{-picoline})_2]$;
III $[Fe(Propox{\cdot}H)_2(Et_2Ph{\cdot}P)_2]$; IV $[Fe(Furox{\cdot}H)_2(Et_2(p\text{-tolyl})P)_2]$;
V $[Fe(D)_3(BOH)_2]{\cdot}4H_2O$; VI $[Fe(Niox)_3(BOCH_3)_2]$
w-weak, s-strong, m-medium

The IR spectral data in Table 2 show strong covalent Fe–N(oxime) and Fe–N(amino) bonds with considerable shifts or splitting of the ν_{C-N}, ν_{N-O} bands as compared to those of the free oximes and amines, respectively.

The characteristic vibrations of the co-ordinated oximes appear approximately at the same frequency values in the spectra of both iron(II)-chelates and clathrochelates.

The ν_{B-O} appear at 1060–1090, 1000–1050 and 800 cm^{-1} and are not sensible for substitution at the boron atom. The $\delta_{Nox-Fe-Nox}$ and $\delta_{Nam-Fe-Nam}$ were found in the spectral range of 310–330 and 270–230 cm^{-1}, respectively, overlapped sometimes by other deformation vibrations (e.g. $\delta_{Nox-Fe-N_L}$, etc.) [10–11].

The Mössbauer spectra of some complexes of above mentioned types have also been recorded [12–15]. In the present paper analogous spectral measurements were carried out with some new derivatives of iron(II). As examples, the data of two dioximine chelates are presented in Table 3.

Table 3 Mössbauer spectral data

Complex	*IS*/mm s^{-1}	*QS*/mm s^{-1}
$[Fe(DH)_2(benzimidazol)_2]$	0.26	1.70
$[Fe(DH)_2(Et_2\text{-}(p\text{-tolyl})P)_2]$	0.13	1.32

Both *IS* (Isomer Shift) and *QS* (Quadrupole Splitting) values characteristic for low spin iron(II) complexes. The *QS* of 1.70 mm s^{-1} is characteristic for *bis*-dioximato-iron(II) complexes. As observed from Table 3, substitution of the axial ligand donor nitrogen atoms for phosphor ones entails the diminution of both *IS* and *QS* values. This indicates the increase of the symmetry in the neighbourhood of the central atom. This effect is due to the possibility of retrodative π-bond formation between the iron(II) central atom and the ligand phosphor atoms, the letter ones having empty *d* orbitals.

Burger *et al.* [13, 15] observed the lack of the correlation between the Mössbauer and positron annihilation parameters. This phenomenon suggests that electrons of the ligands rather than these of the central atom dominate in positron annihilation processes.

Thermal decomposition of the mixed iron(II)-dioximino-chelates and clathrochelates

Toma *et al.* [16–18] have studied the thermal behaviour of some $[Fe(DH)_2L_2]$ complexes (*L*=4-Me-Py, 4-CN-Py, 4-carboxymethyl-Py, imidazol and some pyrazine derivatives) under the conditions of the thermogravimetric analysis in air. The thermal decomposition of these derivatives is a complicated process. In the first stage of the pyrolysis takes place a partial deamination reaction. The loss of the monodentate amine ligand is accompanied by the destruction of the complex moiety in nonstoichiometric and successive reactions. The formation of penta-co-ordinated intermediary product is not excluded.

Unlike to the $[Fe(DH)_2L_2]$ chelates, in the thermal decomposition of the cobalt(III) and rhodium(III) binary salts: $[M(DH)_2L_2]\cdot X$ the loss of the first *L* ligand occurs, generally, in stochiometric ratio:

$$[Co(DH)_2L_2]\cdot X = [Co(DH)_2LX] + L$$

This process has also been studied from kinetic point of view using thermogravimetric methods [19–22].

At higher temperature both the iron(II) and cobalt(III) chelates decomposed following a very complicated mechanism.

Toma *et al.* [16, 17] presume the formation of 2,3-butane-dione as volatile product and 2,3-dimethyl-furazan from the co-ordinated dimethylglyoxime.

We have studied by DSC measurements under argon and nitrogen atmosphere the thermal behaviour of the chelates and clathrochelates of iron(II) characterized in Table 1.

At the decomposition of chelate ring systems the formation of the corresponding α-diketones and substituted or condensed furazan derivatives are not excluded. In order to clear up this problem, during the thermal decomposition some mass spectral and/or gas chromatographic measurements must be carried out.

The thermal decomposition occurs in several successive stages. In the case of crystallohydrates the first stage is a dehydration reaction. In Table 4 one can see some characteristics of this reaction, *viz* the temperature $T_{0.1}$ at which according to the TG curve the transformation degree in the decomposition stage is 0.1, the mass loss Δm in this stage, expressed in moles of H_2O and the temperature T_m corresponding to the endothermal peak on the DSC curve. Obviously, the dehydration is not complete up to the first mass loss stop, but the overall mass loss is consistent with the molecular formula proposed. Since $T_{0.1}$ indicates the beginning of the thermal decomposition, it is normal that the DSC peak temperature T_m is higher than $T_{0.1}$.

Table 4 Dehydration reactions

Complex	$T_{0.1}$/K	ΔM	T_m/K
$[Fe(Diox)_3(BOCH_3)_2]\cdot H_2O$	352	0.95	393
$[Fe(Niox)_3(BOH)_2]\cdot 4H_2O$	308	3.71	325
$[Fe(Glyox\cdot H)_2(\gamma\text{-picoline})_2]\cdot H_2O$	333	0.79	351
$[Fe(Glyox\cdot H)_2(3,4\text{-lutidine})_2]\cdot H_2O$	351	0.85	342

At the thermal decomposition of anhydrous clathrochelates two decomposition stages are observed, although sometimes these steps may overlap each other. The first state exhibits small mass losses, suggesting the loss of BOR, and the second state may be attributed to the destruction of the dioxime ligands. This is why in Table 5 Δm is given in moles of BOR in the case of first stage and in moles of $Diox\cdot H_2$ with the second one. In the same Table the endothermal or exothermal character of the process are indicated as well as the heat of the processes obtained by means of

integrated DSC heat flow curve. In the last column ΔM characterizes the total mass loss, expressed as the % of the 'theoretical' mass loss corresponding to the transformation of the complex into FeO.

As seen from this Table both decomposition processes exhibit an exothermic character. The formation of $Fe(Diox{\cdot}H)_3$ as relatively stable intermediate, might be consistent with our results, but even if it was true, the reaction is not complete. The formation of FeO as a final product remains also only a possibility, since up to 900–1000 K the mass loss is small with the $Niox{\cdot}H_2$ derivatives. In the case of the DH_2 the mass loss is close to the 'theoretical' one, but with these substances the TG curves exhibit a vertical position, indicating a very fast, explosion like decomposition and portions of the sample might be thrown out from the crucible.

Table 5 Decomposition of the clathrochelates $[Fe(Diox)_3(BOR)_2]$

Diox	BOR	$T_{0.1}$/K	Δm/mol	T_m/K	Q/kJ mol^{-1}		ΔM/%
				Stage I			
D	BOH	468	0.66	–	–	–	–
D	$BOCH_3$	438	0.87	482	9.2	exo	–
Niox	BOH	–	–	–	–	–	–
Niox	$BOCH_3$	513	1.21	540	22.5	exo	–
				Stage II			
D	BOH	626	2.82	614	307	exo	93.7
D	$BOCH_3$	588	3.54	589	375	exo	97.3
Niox	BOH	578	2.37	569	242	exo	86.2
Niox	$BOCH_3$	573	1.25	575	194	exo	55.4

The decomposition temperature show a higher thermal stability of DH_2 derivatives as compared to $Niox{\cdot}H_2$ ones, as well as the higher stability of BOR containing clathrochelates as compared to $BOCH_3$ containing ones.

Table 6 shows the thermal decomposition of $[Fe(Diox{\cdot}H)_2(amine)_2]$ type complexes to occur in two stages, which however sometimes, especially with phosphine derivatives, overlap each other.

Presumably, the first stage is a deamination reaction involving the loss of both amine molecules. This process is an endothermic one. Generally it is not complete, but sometimes Δm corresponds to more that 2 amine molecules, i.e. further decomposition process begin already in the first stage. The second stage is an exothermic one, implying also the destruction of the $[Fe(Diox{\cdot}H)_2]$ moiety. It is worth mentioning that this process begins at much lower temperature as compared to the clathrochelates discussed above indicating the high thermal stability of the later ones.

In the case of $[Fe(Propox{\cdot}H)_2(\beta\text{-picoline})_2]$ complex these two stages are followed by a third one corresponding to $T_{0.1}$=843 K and exhibiting a mass loss of Δm=0.44 moles of $Propox{\cdot}H_2$.

Table 6 Decomposition of the $[Fe(Diox{\cdot}H)_2L_2]$ type chelates

Diox·H	Ligand	$T_{0.1}$/K	Δm/mol	T_m/K	G/kJ mol^{-1}		ΔM%
				Stage I			
Glyox·H	γ-picoline	420	1.30	417	37.3	endo	–
Glyoox·H	3,4-lutidine	423	1.40	420	43.4	endo	–
DH	pyridine	461	2.62	464	19.6	endo	–
DH	Et_2(*p*-tolyl)P	460	2.48	–	–	–	–
Propox·H	γ-picoline	455	2.40	447	170	endo	–
Propox·H	β-picoline	412	1.58	425	90.4	emdp	–
Propox·H	Et_2PhP	451	1.69	435	5.1	exo	–
Furox·H	Et_2PhP	489	3.04	477	81.1	emdo	–
Furox·H	Et_2(*p*-tolyl)P	475	2.90	458	41.1	endo	–
				Stage II			
Glyox·H	γ-picoline	475	2.01	483	247	exo	98.3
Glyox·H	3,4-lutidine	478	2.50	480	187	exo	104.2
DH	pyridine	496	0.80	484	296	exo	90.0
DH	Et_2(*p*-tolyl)P	–	–	494	442	exo	85.5
Propox·H	γ-picoline	473	1.70	481	334	exo	104.2
Propox·H	β-picoline	471	1.57	481	774	exo	97.1
Propox·H	Et_2PhP	501	1.05	486	311	exo	77.0
Furox·H	Et_2PhP	–	–	507	136	exo	78.8
Furox·H	Et_2(*p*-tolyl)P	–	–	512	264	exo	74.2

Concerning the final product the last column of Table 6 may give some information. As seen sometimes ΔM depasses the theoretical mass loss corresponding to the formation of FeO. Therefore one can be sure that some material was thrown out from the sample holder during the explosion like very fast second decomposition stage. On the TG curve vertical portions appear in these cases and also with substances exhibiting ΔM values higher than 90% of the 'theoretical' mass loss. Such vertical portions are absent only with phosphine derivatives, but in these cases up to 900–950 K ΔM is only about 80% of the 'theoretical' one. Thus the final product of the phosphine derivatives can not be FeO. In the case of the pyridine derivatives our above results are not inconsistent with the presumption that the final product is FeO.

$T_{0.1}$ and T_m data presented in Table 6 indicate also the high stability of the furox·H_2 derivatives. This might be assigned to the more extended delocalized π-bond system of the $[Fe(Furox{\cdot}H)_2]$ moiety as compared to the complexes containing other dioximes. This effect is similar to that observed with diphenylglyoximine complexes of cobalt(III) $[Co(Diph{\cdot}H)_2L_2]{\cdot}X$ [23].

With respect to the gaseous products evolved we have only presumptions. At the beginning the coordinated amine may be liberated.

In the case of several decomposition stages the shape of the TG curve allowed us to derive some kinetic parameters as apparent reaction order *n*, activation energy *E*, and pre-exponential factor *A*. For this purpose our nomogram method have been used [24]. This method is based on the empirical correlation between *n*, *E* and *A* and some reduced 'shape' and 'position' parameters.

The shape ∇, Δ and the position parameters τ are defined as:

$$\nabla = \frac{\theta_{0.5} - \theta_{0.9}}{\theta_{0.1} - \theta_{0.9}}; \qquad \Delta = 10^6(\theta_{0.1} - \theta_{0.5}); \qquad \tau = 10^5\theta_{0.1} \tag{1}$$

where $\theta = T_\alpha^{-1}$ and T_α stands for the temperature at which in the decomposition stage considered the conversion attains the value α.

The reduced parameters ∇^x and Δ^x and τ^x are correlated with the parameters given by (1) according to the following relations:

$$\nabla^x = \nabla + N_1 Q_1 L_1^{-1}(\lg E - Q_2)^{-1} \tag{2}$$

$$\Delta^x = \left\{\Delta + [7.1 - 5(\lg E - 6)Q_6 L_2^{-1} E^{-1}]\right\}[N_2 - N_3 Q_7(4 + 3\lg A)^{-1}(\lg E - 1)^{-1}]^{-1} \tag{3}$$

$$\tau^x = \tau + [101n + Q_5 - (Q_3 n + Q_4)(4 + lgA)^{-1}]E^{-1} \tag{4}$$

$$Q_1 = 1.42(6 - \lg q)\cdot 10^{-2}[6.9 - 3\lg q + 0.45(\lg q)^2]^{-1}$$

$$Q_2 = (6 + \lg q)3^{-1}$$

$$Q_3 = 16.6(\lg q + 4.39)$$

$$Q_4 = 300(\lg q + 0.778)(\lg q + 11.75)$$

$$Q_5 = 4550(\lg q + 0.778)$$

$$Q_6 = [2.443 + 3.473\lg q + 0.428(\lg q)^2]10^4$$

$$Q_7 = [1.353 + 0.535\lg q + 0.103(\lg q)^2]10^{-3}$$

$$N_1 = 1 + 0.6n + 0.25n^2$$

$$N_2 = 1 + 0.16n + 0.011n^2$$

$$N_3 = 12n(n + 3)$$

$$L_1 = 1 + 0.5\lg A + 0.07(\lg A)^2$$

$$L_2 = 4 + 1.5\lg A + 0.16(\lg A)^2$$

The above given formulas are valid if the heating rate q is expressed in K s^{-1}, the apparent activation energy E in cal/mol and the apparent pre-exponential factor in s^{-1}.

The shape parameter is correlated with the apparent reaction order according to the relation [25]

$$n = 6.182 - (62.579 - 90.91\nabla^x)^{1/2} \quad (5)$$

E and A are unique functions of the reduced parameters τ^x and Δ^x . Their correlation is given in a nomogram published earlier.

In order to apply this method, we determined the temperatures $T_{0.1,}$ $T_{0.5}$ and $T_{0.9}$ by using the corresponding portion of the TG curve and we calculated the shape and position parameters by means of formulae (1).

Let us consider as an example the first decomposition stage of $[Fe(Furox{\cdot}H)_2(Et_2PhP)_2]$. The characteristic temperatures are: $T_{0.1}$=489 K; $T_{0.5}$=519 K; $T_{0.9}$=540 K.

The shape and position parameters calculated by means of relations (1) are the following: ∇=0.3880; Δ=118.21; τ=2.0450.

From the shape parameter the first approach for the reaction order is calculated by introducing ∇ into (5).

One obtains: n_1=0.96

Since for the calculation of the reduced parameters both E and A must be known, we apply an iterative procedure. In the first cycle instead of (5) we used the approximation

$$\Delta_1^x = \Delta N_2^{-1}$$

N_2, calculated with the above given n_1 value is equal to 1.1657, thus Δ_1^x =101.58 is obtained. By taking $\tau_1^x = \tau$, the first approach for E and A can be taken from the nomogram. The above co-ordinates determine the point P in Fig. 1, representing a portion of the nomogram. This point is situated between the iso-activation energy curves corresponding to E=28 kcal and E=30 kcal, and between the curves lg$A$=10 and lg$A$=11. E_1 and A_1 values can be obtained by means of a non-linear interpolation.

Let us consider two neighbouring iso-activation energy curves corresponding to X and Y kcal, respectively. By constructing a vertical straight line passing through P, one can measure the distance a between the curve X and the point P, as well as the distance b between P and Y. The ratio D_L=a/(a+b) would allow a linear interpolation: $E=X+D_L(Y-X)$, but this can not be correct. Let us denote the correct interpolation formula as: $E=X+D(Y-X)$. The correlation between D and D_L is given in Fig. 2.

The same curve can be used in order to perform a non-linear interpolation between two neighbouring lg$A$=const. curves, by constructing a horizontal straight line for determining the ratio D_L. In our example a/(a+b)=0.775 corresponding to D=0.695, c/(c+d)=0.252 corresponding to D=0.182 as indicated in Fig. 2 with dashed lines.

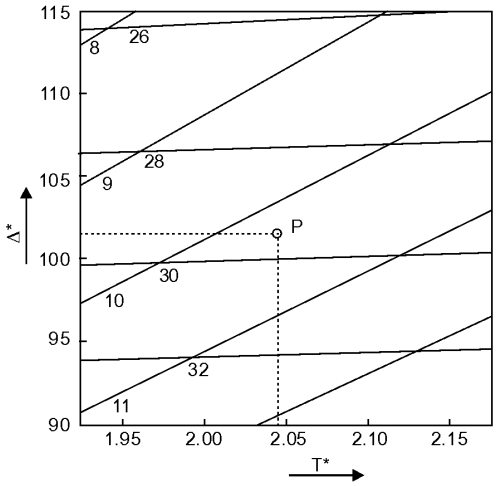

Fig. 1 Portion of the E – lg$A$ nomogram

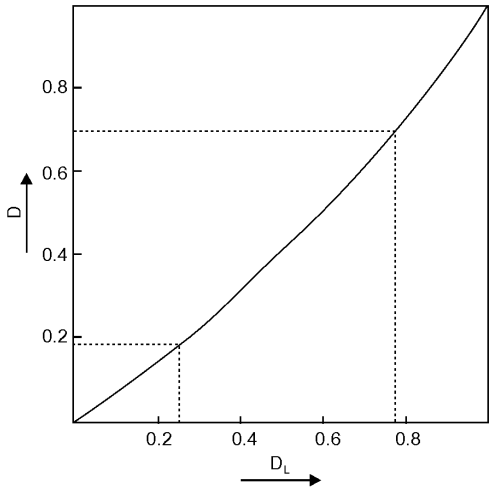

Fig. 2 Diagram for non-linear interpolation

Consequently, one obtains, E_1=29.39 kcal and lgA_1=10.18

In the second iterative cycle Δ_1^x is calculated by using n_1, E_1 and lgA_1 values and Eq. (2). By introducing ∇_1^x into (5) one obtains n_2. By using relations (3) and (4), the obtained n_2, E_1 and lgA_1 values yield Δ_2^x and τ_2^x, which will be the co-ordinates of the point P_1 in the nomogram. By means of non-linear interpolation one obtains the corresponding E_2 and lgA_2. Thus one obtains: ∇_1^x=0.3885, n_2=0.96, Δ_2^x=101.58, τ_2^x=2.0482, E_2=29.40 and lgA_2=10.20.

Obviously, these results are practically identical with those obtained in the previously iteration cycle. This is a consequence of the use of the heating rate

q=10 K min^{-1}, which has been the standard heating rate at the construction of the nomogram and implying Q_4=Q_5=Q_6=0.

By using other heating rates, the differences between the first and the second approaches are larger, but even in these cases the approximations of higher order are always almost identical with the second one. The results obtained by means of the above procedure are presented in Table 7.

Table 7 Kinetic parameters derived for some decomposition stages of the [Fe(Diox·H)$_2$L$_2$] type chelates

Diox·H	Ligand	Stage	τ	n	E/kJ mol^{-1}	lg$A$	lgA'
Glyox·H	γ-picoline	I	2.3809	2.49	192.8	21.50	21.40
Glyox·H	3,4-lutidine	I	2.3641	1.88	228.3	25.63	25.68
Propox·H	β-picoline	I	2.4272	0.29	101.7	10.06	10.05
Propox·H	β-picoline	III	1.1862	2.66	708.0	41.33	41.26
Propox·H	γ-picoline	I	2.1978	1.27	258.6	27.04	27.17
Propox·H	Et_2PhP	I	2.2173	2.18	127.1	11.97	11.90
Furox·H	Et_2PhP	I	2.0450	0.96	123.1	10.20	10.24
Furox·H	Et_2(*p*-tolyl)P	I	2.1053	0.95	116.1	9.85	9.86

The last column of the Table 7 contains the lgA' values. A' may be considered as a 'theoretical' pre-exponential factor, resulting from the correlation between A, E and τ reported earlier [27], and which expresses the so-called kinetic compensation effect in the TG kinetics. This correlation is given as

$$\lg A' = \frac{\tau E'}{R\ln 10} + \lg(qE'\tau^2) - 4.85 \qquad (6)$$

where E' stands for the activation energy expressed in kJ mol^{-1}, q is given in K s^{-1} and A' in s^{-1}.

As seen from Table 7, lgA' values calculated by using Eq. (6) are in good agreement with lg$A$ values derived from the TG curves by using the nomogram method. These results prove the validity of relation (6).

Experimental

[Fe(Diox·H$_2$)L$_2$] type complexes

From the solutions of 10 mmol $Fe(NH_4)_2(SO_4)_2{\cdot}6H_2O$ in 80–100 cm^3 water and of 20 mmol α-dioxime and 30 mmol amine (phosphine) in 100 cm^3 ethanol, respectively, air was removed by bubbling nitrogen or methane. The mixture of the solutions was stirred 10–20 min under nitrogen atmosphere. The separated crystalline products were filtered off, washed with dil. alcohol and dried in air. Yield: 70–80%.

[Fe(Diox)$_3$(BOH)$_2$]·nH$_2$O

5 mmol $FeCl_2 \cdot 4H_2O$, 5 mmol ascorbic acid in 50 cm^3 water were treated with 15 mmol α-dioxime, 50 mmol boric acid and 5–10 mmol borax (or sodium acetate) in 25–30 cm^3 water (pH=approx. 3). After 15–20 min stirring the mixture, the separated crystalline product was filtered off, washed with cold water and dried on air. Yield: 60–70%.

[Fe(Diox)$_3$(BOR)$_2$]

The mixture of 5 mmol $FeCl_2 \cdot 4H_2O$, 15 mmol α-dioxime and 25–30 cm^3 methanol were stirred for 10 min, treated with 10 mmol H_3BO_3 and boiled under reflux for an additional 10–15 min. Then 2.5 mmol borax was added slowly to the warm, dark solution. After boiling again for 15–20 min, the solid product formed was filtered off, washed with diethylether or petrolether. The product was recrystallized from alcohol or acetonitril. Yield: 40–50%.

Analysis

The iron content of the samples was determined gravimetrically as Fe_3O_4, or complexometrically with EDTA, after destroy of the samples with boiling H_2SO_4 and some crystals of KNO_3. Nitrogen content was determined by standard microanalytical method.

The far IR spectra were measured with Bio-Rad-Ninn spectrometer in polyethylene pellets while the middle FTIR ones with Perkin Elmer 2000 apparatus in KBr pellets.

The thermal measurement were carried out with a 951-TG and 910-DSC calorimeter (DuPont Instruments) in argon and nitrogen atmosphere. Sample mass: 5–6 mg, heating rate 10 K min^{-1}.

* * *

One of us (Cs. V.) would like to thank the Foundation 'Pro Renovanda Hungaria', 'Guest Professors in Hungary' for providing one month fellowship to Hungary (1997). This work was financially supported by Hungarian Research Foundation (grant OTKA T022909 and T-19555). The authors thank to Prof. K. Burger for helpful discussion concerning interpretation of Mössbauer spectra.

References

1 K. Burger, L. Korecz, J. B. A. Manuaba and P. Mag, J. Inorg. Nucl. Chem., 28 (1966) 1675.
2 J. Zsakó, J. Horák and Cs. Várhelyi, Rev. Roum. Chim., 26 (1981) 1271.
3 J. Zsakó, Cs. Várhelyi and T. Sasvári, Stud. Univ. Babes-Bolyai, Chem., 34 (1989) 10.
4 J. Horák, Z. Pinta and Cs. Várhelyi, J. Inorg. Nucl. Chem., 45 (1981) 111.
5 L. A. Chugaev, Z. Anorg. Allg. Chem., 46 (1905) 144.
6 S. C. Jackels and N. J. Rose, Inorg. Chem., 12 (1973) 1252.
7 J. N. Johnson and N. J. Rose, Inorg. Synth., 21 (1982) 112.

8 M. K. Robins, B. N. Nase, J. L. Heilend and I. J. Grzybowski, Inorg. Chem., 24 (1985) 3381.
9 Ya. Voloshin, N. A. Kostromina and A. Yu. Nazarenko, Inorg. Chim. Acta, 170 (1990) 182.
10 K. Nakamoto, Infrared and Raman Spectra of Inorganic and Coordination Compounds, 3rd, Wiley, New York 1978.
11 J. R. Ferraro, Low-Frequency Vibrations of Inorganic and Coordination Compounds, Plenum Press, New York 1971.
12 A. V. Ablov, V. I. Goldanskii, R. A. Stukan, K. J. Turta and B. N. Zubarev, Dokl. Akad. Nauk SSSR, 170 (1966) 128.
13 L. Korecz, A. A. Saghier, Cs. Várhelyi and K. Burger, Acta Chim. Acad. Sci. Hung., 101 (1979) 27.
14 Z. Kajcsos, A. Vértes, G. Brauer, L. Marczis, Cs. Várhelyi and K. Burger, J. Cryst. and Spectroscop. Res., 13 (1983) 431.
15 A. Vértes, K. Burger, T. Tarnóczy, E. Papp-Molnár and C. L. Egyed, Acta Chim. Acad. Sci. Hung., 59 (1969) 15.
16 H. E. Toma and L. A. Morino, Trans. Met. Chem., 15 (1990) 66.
17 H. E. Toma and L. A. Morino, J. Thermal Anal., 36 (1990) 7.
18 H. E. Toma, A. M. Ykenti, M. C. Silva and L. A. Morino, Quim. Nova, 12 (1989) 295: Chem. Abstr., 114 (1991) 94107.
19 J. Zsakó, J. Horák and Cs. Várhelyi, J. Thermal Anal., 20 (1981) 435.
20 J. Zsakó, J. Horák, Cs. Várhelyi and A. Benkő, Monatsh. Chem., 112 (1981) 945.
21 J. Zsakó, E. Kékedy and Cs. Várhelyi, Rev. Roum. Chim., 19 (1970) 865.
22 J. Zsakó, E. Kékedy and Cs. Várhelyi, J. Inorg. Nucl. Chem., 32 (1970) 2999.
23 J. Zsakó, E. Kékedy and Cs. Várhelyi, Stud. Univ. Babes-Bolyai, Chem., 14 (1969) 117.
24 J. Zsakó, J. Thermal Anal., 15 (1979) 369.
25 J. Zsakó, G. Marcu and Cs. Várhelyi, Rev. Roum. Chim., 27 (1982) 815.
26 J. Zsakó, M. Várhelyi and Cs. Várhelyi, J. Thermal Anal., 17 (1979) 123.